

Moulding and shielding flexural waves in elastic plates

T. Antonakakis^{1,2}, R. V. Craster², S. Guenneau³

¹ *European Organization for Nuclear Research, CERN CH-1211, Geneva 23, Switzerland*

² *Department of Mathematics, Imperial College London, London SW7 2AZ, UK and*

³ *Institut Fresnel, UMR CNRS 6133, University of Aix-Marseille, Marseille, France*

Platonic crystals (PCs) are the elastic plate analogue of the photonic crystals widely used in optics, and are thin structured elastic plates along which flexural waves cannot propagate within certain stop band frequency intervals. The practical importance of PCs is twofold: these can be used either in the design of microstructured acoustic metamaterials or as an approximate model for surface elastic waves propagating in meter scale seismic metamaterials. Here, we make use of the band spectrum of PCs created by an array of very small clamped circles to achieve surface wave reflectors at very large wavelengths, a flat lens, an endoscope, a directive antenna near stop band frequencies and cloaking from Dirac-like cones. The limit as the circles reduce to points is particularly appealing as there is an exact dispersion relation available so the origin of these phenomena can be explained and interpreted using Fourier series and high frequency homogenization.

There has been much interest over the past 20 years in the analysis of elastic waves in thin plates in the continuum mechanics community [1, 5, 21, 30, 32, 33, 35]; an interest renewed in the metamaterial community with the theoretical proposals [4, 13, 14, 16], and their subsequent experimental validation [6, 38, 40], of broadband cloaks and negatively refracting flat lenses for flexural waves.

One of the attractions of platonic crystals is that much of the physics of photonic crystals can be translated into platonic crystals (PCs). There are mathematical subtleties in the analysis, and numerics, of the scattering of flexural waves [35] owing to the fourth-order derivatives, versus the usual second-order derivatives for the wave equation of optics, involved in the governing equations; even the waves within a perfect plate have differences from those of the wave equation as they are not dispersionless.

There is a long history of wave propagation along periodically supported plates motivated by ribbed structures in underwater acoustics, [31]; the periodically constrained plate [30] being considered in detail. Movchan et al. [32] also give a complementary treatment for the flexural plate containing square arrays of circular holes or clamped circles using lattice sums and multipoles with a dilute limit giving approximate dispersion relations in closed form. Fourier series expansions introduced in [12, 30] and applied in [5] also allow for a highly accurate analytic expression for the exact dispersion equation for plates when the radius of the clamped circles tends to zero and the clamping is at points. We follow this latter route, which combined with the recently developed high frequency homogenization theory (HFH) [11], uncovers the physics of point clamped plates; a striking illustration (lensing) is shown in Fig. 2(b), which contrasts with a shielding effect at a lower frequency in Fig. 2(a). The latter obviously has potential application in seismic metamaterials [8] for anti-earthquake systems.

Much has been said about control of light [37], sound, water, or shear (SH) waves [9] using the rich behaviour encapsulated by the dispersion curves of bi-periodic

structures, modelled by a Helmholtz equation, up to minor changes in the normalization of material parameters, and choice of boundary conditions (e.g. Dirichlet or Neumann for clamped or freely vibrating inclusions in the context of SH waves). However, when one moves into the area of elastic waves, governed by Navier equations, it is no longer possible to reduce the analysis to a single scalar partial differential equation (PDE), as shear and pressure waves do couple at boundaries. There is nevertheless, the simplified framework of the Kirchhoff-Love plate theory [17] that allows for bending moments and transverse shear forces to be taken into account via a fourth-order PDE for the out-of-plane plate displacement field. This plate theory is a natural extension of the Helmholtz equation to a generic model for flexural wave propagation through any spatially varying thin elastic medium. It offers a very convenient mathematical model for any physicist wishing to grasp (some of) the physics of PCs using earlier knowledge in photonic or phononic crystals. However, while the Helmholtz equation can, with appropriate notational and linguistic changes, hold for acoustic, electromagnetic, water or out-of-plane elastic waves and so encompasses many possible applications, the Kirchhoff-Love plate theory is dedicated to the analysis of flexural waves. For instance, it says little about propagation of in-plane elastic waves in platonic crystals.

Flexural, also called bending, waves are fundamentally different in character from compressional acoustic or electromagnetic waves; they model the lowest frequency waveguide mode for elastic waves and therefore are dispersive. For these low frequencies, equivalently thin plates, the phase and group velocities scale with square root of the frequency and this is reflected in the model equations which are fourth order in space and second order in time. A reduced model is derived in [17, 26] for flexural waves, and in the frequency domain it is

$$\left(\frac{\partial^2}{\partial x_1^2} + \frac{\partial^2}{\partial x_2^2} + \Omega \right) \left(\frac{\partial^2}{\partial x_1^2} + \frac{\partial^2}{\partial x_2^2} - \Omega \right) u = 0, \quad (1)$$

for $u(x_1, x_2)$ on the square cell $-1 < x_1, x_2 < 1$ where this has been non-dimensionalised: All results presented are in non-dimensional units and one can return to the dimensional setting using that $\Omega^2 = 12(1 - \nu^2)\rho\omega^2/(Eh^2)$, where ρ , h , E , ν are density, thickness, Young's modulus and Poisson's ratio of the plate, respectively, and ω is the angular wave frequency; the plate contains a square array of very small clamped circles, so both $u = 0$ and $\partial u/\partial r = 0$ on, and within, a radius $r = a$ centred at each lattice point of the array.

In the context of optics, (1) reduces to a second order PDE where only the first factor of (1) appears, in which case Dirichlet boundary conditions are a good model for infinite conducting thin wires at GHz frequencies, with the unknown u of such a Helmholtz equation being the longitudinal component of the electric field E_z in TM polarization and the spectral parameter Ω is associated with $\omega^2\varepsilon(x_1, x_2)/c^2$ whereby ω is the electromagnetic wave frequency, ε is the relative permittivity and c is the speed of light in a vacuum. Such a model has been known since the mid 90s to lead to a zero frequency stop band associated with very low frequency plasmons [34, 36].

For waves propagating through an infinite PC containing a square array of identical defects, one can invoke Bloch's theorem [7, 24] and simply consider a square cell of sidelength 2 with Bloch conditions applied to the edges. The Bloch wave-vector $\boldsymbol{\kappa} = (\kappa_1, \kappa_2)$ characterizes the phase-shift going from one cell to the next. Applying the clamped boundary conditions at the local origin at each lattice point, leads to an exact solution when the cylinder radius shrinks to a point, as readily found [5, 30] which gives the dispersion relation $D(\boldsymbol{\kappa}, \Omega) = 0$ where

$$D(\boldsymbol{\kappa}, \Omega) = \sum_{n_1, n_2 = -\infty}^{\infty} \frac{1}{[(\pi n_1 - \kappa_1)^2 + (\pi n_2 - \kappa_2)^2]^2 - \Omega^2}. \quad (2)$$

As is well-known in solid state physics [7] only a limited range of wavenumbers need normally be considered, namely the wavenumbers along the right-angled triangle ΓXM shown in the irreducible Brillouin zone inset in Fig. 1. There are however some exceptions, where it is possible to miss important details such as the stop band minima/maxima not occurring at the edges of the Brillouin zone [2, 3, 20] and flat bands leading to strong anisotropy and slow light [10].

The dispersion diagram is shown in Fig. 1; the singularities of the summand in Eq. (2) correspond to solutions within a square cell (without the clamped array) satisfying the Bloch conditions at the edges, in some cases these singular solutions also satisfy the conditions at the support and are therefore true solutions to the problem. Solid lines in Fig. 1 are the dispersion curves double checked by the finite element method (FEM) using the commercial package Comsol, notable features are the zero-frequency stop-band and also crossings of branches at the edges of the Brillouin zone. Importantly,

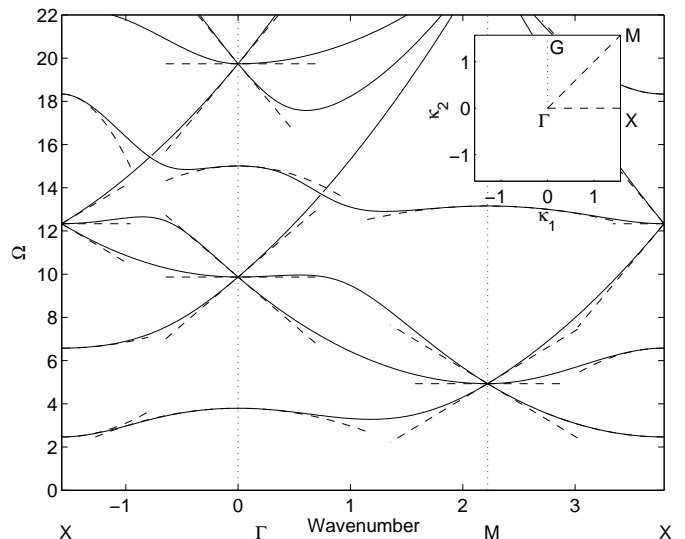


Figure 1: Bloch dispersion curves around the edges of the Brillouin zone ΓXM (inset) for an array of clamped circles (radius 0.01) of pitch 2. One notes the stop band for $\Omega \in [0, \pi^2/4]$ and three Dirac-like cones at frequencies $\Omega = \pi^2/2$ (X point), π^2 and $2\pi^2$ (Γ point). Solid curves are computed with FEM, and dashed curves are from HFH.

HFH [5] captures the physics of this band diagram, with the asymptotic theory giving dashed curves that fit very well with the FEM (solid curves) near the band-gap edges which are the zero-group velocity and Dirac-like cones. The multiple scales used for HFH are a short-scale $\xi_i = x_i/l$ and a long-scale $X_i = x_i/L$ for $i = 1, 2$ where l and L represent respectively the characteristic small scale (half length of a cell) and the long scale. A small parameter is formed as $\epsilon = l/L$ and an expansion of $\Omega^2 = \Omega_0^2 + \epsilon\Omega_1^2 + \dots$ and $u = u_0 + \epsilon u_1 + \dots$ is posed with respect to this parameter. Here Ω_0 is a standing wave frequency given at the points X , Γ and M and a perturbation scheme can be developed about the band edges. The leading order term for u is $u_0(\boldsymbol{\xi}, \mathbf{X}) = f_0(\mathbf{X})U_0(\boldsymbol{\xi})$ where the function f_0 representing an envelope of the solution u is obtained by an equation only on the long scale: The theory is detailed in [5]. Changing back to the original x_i coordinates the effective medium equation [5] reads,

$$T_{ij} \frac{\partial^2 f_0}{\partial x_i \partial x_j} - \frac{(\Omega^2 - \Omega_0^2)}{l^2} f_0 = 0. \quad (3)$$

T_{ij} 's are integrated quantities of the leading order and first order short scale solutions with $T_{ij} = 0$ for $i \neq j$ in the present illustrations. As in [5], assuming Bloch waves, the asymptotic dispersion relation for Ω reads,

$$\Omega \sim \Omega_0 - \frac{T_{ij}}{2\Omega_0} \kappa_i \kappa_j, \quad (4)$$

where $\kappa_i = K_i - d_i$ and $d_i = 0, -\pi/2, \pi/2$ depending on the band edge in the Brillouin zone about which the

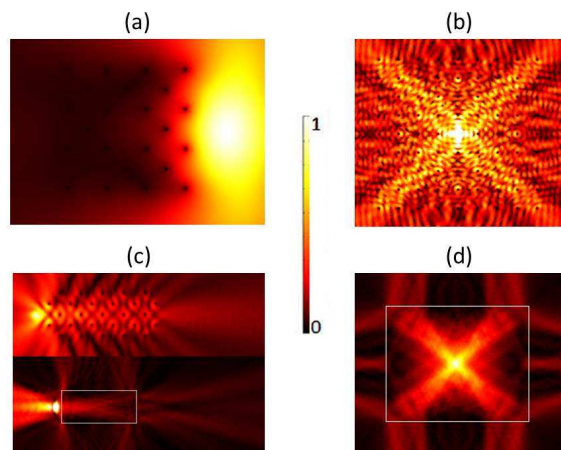


Figure 2: (a) A forcing generates a bending wave totally reflected by the array (with 22 clamped circles), throughout the zero-frequency stop band of Fig. 1 (here $\Omega = 2$). From the four-fold symmetry of the array and linearity of Eq.1, the defect at the center of the array (one missing circle) is shielded from the bending waves. (b) A point source placed in the centre of an array of 80 circles of radius 0.01 in a regular square orientation at the same frequency of $\Omega = 6.58$ produces a X shape. (c) An endoscope effect of bending wave excited by a point forcing of normalized frequency $\Omega = 6.58$ through an array (pitch 2) of 27 clamped circles (radius 0.01) tilted through an angle $\pi/4$. (d) Represents the same X shape effect produced by an effective material created by Eq. (3) with $T_{11}T_{22} < 0$ yielding characteristic type of solutions. Panels (b) and (d) use the PC array in the usual ΓX symmetry direction whereas panels (a), (d) rotate the array to use the ΓM symmetry direction.

asymptotic expansion originates, and Ω_0 is the standing wave frequency at the Brillouin zone edge ; these asymptotics give the dashed curves in Fig. 1. For the case of multiple modes originating from the same point, as for example the Dirac-like cones, Eq. (4) is no longer valid and one obtains three coupled equations for $f_0^{(i)}$ that simplify to three similar isotropic equations, like (3) with $T_{11} = T_{22}$. Note that Eq. (3) is of second order and not fourth. The fourth order plate equation yields two types of solutions namely propagating and exponentially decaying. Indeed in the long scale, solutions follow a second order PDE and the remaining information of the fourth order problem is enclosed in the T_{ij} integrated quantities. This homogenization theory is not limited to long-waves relative to the microstructure, one apparent failing is that the asymptotics appear to be only valid near the band edge frequencies but further refinements are possible, using foldings of the Brillouin zone, that extend the theory to provide complete coverage of the dispersion curves and provide accuracy at all frequencies.

We give three potential applications of the platonic crystal described by Fig. 1. A finite array of the PC is embedded within an infinite elastic plate and the full

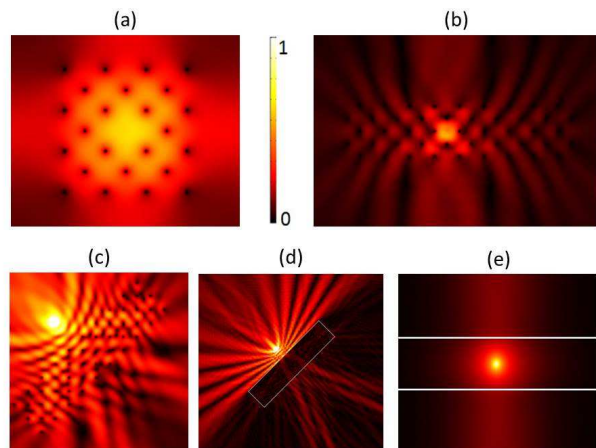


Figure 3: A bending wave excited by a forcing of normalized frequency $\Omega = 3.7952$ (that of vanishing group velocity at Γ point in Fig. 1) inside an array of clamped circles (pitch 2, radius 0.01) tilted through an angle $\pi/4$ gives rise to respectively four (a) and two (b) highly-directed beams outside 24 circles making a square (a) and 47 circles making a rectangle (b). Focusing through a slab of 48 circles is shown in (c) with its HFH equivalent in (d) for a point forcing at normalized frequency of $\Omega = 6.58$. The focusing (d) and antenna (e) effects are simulations of the continuum PDEs (3) generated by HFH with respective (T_{11}, T_{22}) coefficients of $(25.65, -11.18)$ at point X and $(6.2524, 6.2524)$ at point Γ , where the effective media are highlighted by white lines. Panels (a) and (b) use the PC array in the ΓM symmetry direction and panel (c) uses the ΓM symmetry direction.

finite element simulations (making use of specially designed perfectly matched layers [15] are compared to solutions constructed using the continuum long-scale HFH theory to replace the finite array; standard continuity conditions then join this HFH material to the surrounding infinite elastic plate. This theory captures a rich array of behaviour, for instance the material displays strong anisotropy with propagation along characteristics in Fig. 2(b) that is well captured by HFH in Fig. 2(d); the coefficients T_{ij} of the HFH theory are of opposite sign ($T_{11} = 25.65$ and $T_{22} = -11.18$) and capture the strong anisotropy of the medium and the effective material becomes hyperbolic rather than elliptic, which unveils the similar lensing effect without negative refractive index to that observed in [29]. Also shown in Fig. 2(a) are the shielding effect of the zero frequency stop band and strong guiding of energy within a PC slab Fig. 2(c).

Using the vanishing group velocity of the second dispersion curve in Fig. 1, in the neighborhood of Γ , a strongly directive antenna is created as shown in Fig. 3(a,b) and (e). The effective medium for the directive antennas is governed by Eq. (3) with $T_{11} = T_{22} = 6.2524$. Fig. 3(c) and (d) shows an endoscope effect wherein a point source located close to a tilted array leads to fo-

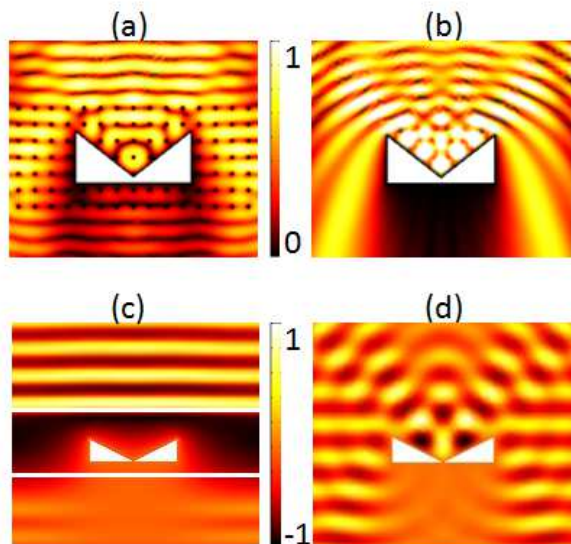


Figure 4: A plane bending wave of normalized frequency $\Omega = 9.7$ (just below the first Dirac-like cone at Γ point in Fig. 1) incident from the top on an array of clamped circles (pitch 2, radius 0.01) undergoes considerably less scattering (a) than by a clamped obstacle on its own (b); panels (a,b) are from finite element simulation. The asymptotic HFH PDEs from equation (5) capture the essence of physics, and the equivalent results are shown for cloaking (c) and scattering (d) by the same clamped obstacle.

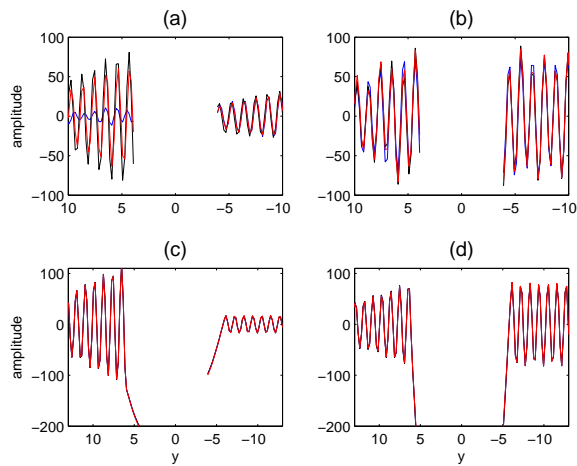


Figure 5: Shape independence for three obstacles of same area, namely a square, $\pi/4$ tilted square and a circle in the same setting as in Fig. 4. (a) and (b) plot forward and back scattering on the respective paths $x = 0$ and $x = 15$ (outside the obstacle abscissa) for three different obstacle shapes without any periodic medium. (c) and (d) plot forward and back scattering on the same paths only this time with an effective medium that surrounds the obstacle just like in Fig. 4(c).

cussing and a strong localised beam. The behaviour near point M of the Brillouin zone is responsible for the fo-

cussing effects of Fig. 2(b) and Fig. 3(c). Here the closest standing wave frequency is at point M and unequal T_{ii} coefficients lead to very strong anisotropy within the effective material. By considering only a portion of the Brillouin zone we must bear in mind that this asymptotic solution is also valid at N and there is a second f equation with the T_{11} and T_{22} interchanged that is used. The asymptotic PDE for HFH is Eq. (3) with $T_{11} = -9.649$ and $T_{22} = -4.935$. Ω_2 is determined using the the frequencies stated in Figs 2(b), 3(c) and the standard expansion for Ω .

Last, but not least, the triple crossings in the dispersion diagram in Fig. 1 comprise Dirac-like cones with a flat mode passing through the vertex. This is highly interesting given that Dirac-like cones are normally limited to graphene-like hexagonal structures [19]; the current situation involves a square lattice is akin to the Dirac-like cones for photonic crystals recently described in [22, 28]. One can use the properties of Dirac cones-like to reduce the scattering of a clamped obstacle in a PC, as demonstrated in Fig. 4(a),(b). This behaviour is also captured by HFH asymptotics: In this particular case three coupled equations emerge with variables $f_0^{(i)}$ for $i = 1, 2, 3$. The system decouples to yield the same governing equation for all three functions $f_0^{(i)}$ as,

$$8\pi^6 \frac{\partial^2 f_0}{\partial x_i^2} + \frac{(\Omega^2 - \Omega_0^2)^2}{l^2} f_0 = 0, \quad (5)$$

where the coefficient in front of f_0 comes from first order correction Ω_1 and the change into the original coordinates; the numerics using HFH are shown in Fig. 4(c). The front and back scattering do not depend on the shape of the obstacle but mostly on its area. Fig. 5(c) and (d) show the scattering of three different obstacles (a square, a tilted square and a circle) are virtually indistinguishable, whereas in panels (a) and (b) the three curves can be clearly told apart. The platonic crystal is used to destroy any one-to-one correspondence between the scattered field and the shape of an obstacle, which is the essence of cloaking in impedance tomography [18, 25]. However, we note that the present cloaking is constrained to normal incidence and is reminiscent of [39] which is a more elaborate type of cloaking somewhat constrained to the eikonal limit of transformation optics with photonic band gap media [27].

In conclusion, a simplified model of elasticity via the thin-plate equation allows for analytical and numerical studies opening interesting possibilities in the design of flat lens, directive antenna, endoscope, shielding and a cloak for flexural waves. Moreover, such designs could be scaled up in order to achieve some control of seismic surface waves [8], [23], indeed this work is motivated by a requirement at CERN to control elastic waves created by thermal shock. We also show, for the first time, that the computations using the recently developed HFH are

capable of capturing the fundamental wave propagation features of these various possibilities, including counter-intuitive physics of Dirac-like cones [28].

R.V.C. thanks the EPSRC (UK) for support through research grant number EP/J009636/1. S.G. is thankful for an ERC starting grant (ANAMORPHISM).

-
- [1] Abrahams, I. D., and A. N. Norris (2000), Proc. R. Soc. Lond. A **456**, 1559.
- [2] Adams, S. D. M., R. V. Craster, and S. Guenneau (2008), Proc. R. Soc. Lond. A **464**, 2669.
- [3] Adams, S. D. M., R. V. Craster, and S. Guenneau (2009), Waves in Random and Complex Media **19**, 321.
- [4] Al-Lethawe, M. A., M. Addouche, A. Khelif, and S. Guenneau (2012), New J. Phys. **14**, 123030.
- [5] Antonakakis, T., and R. V. Craster (????), Proc. R. Soc. Lond. A **468**, 1408.
- [6] Bonello, B., L. L. Belliard, J. Pierre, J. O. Vasseur, B. Perrin, and O. Boyko (2010), Phys. Rev. B **82**, 104109.
- [7] Brillouin, L. (1953), *Wave propagation in periodic structures: electric filters and crystal lattices*, 2nd ed. (Dover, New York).
- [8] Brule, S., E. Javelaud, S. Guenneau, S. Enoch, and D. Komatitsch (2012), in Proceedings ETOPIIM 9 (Marseille, September 2-7), Ed. S. Enoch and S. Guenneau.
- [9] Craster, R., and S. Guenneau (2012), *Acoustic metamaterials: Negative refraction, imaging, lensing and cloaking* (Springer Verlag, London).
- [10] Craster, R. V., T. Antonakakis, M. Makwana, and S. Guenneau (2012), Phys. Rev. B **86**, 115130.
- [11] Craster, R. V., J. Kaplunov, and A. V. Pichugin (2010), Proc R Soc Lond A **466**, 2341.
- [12] Evans, D. V., and R. Porter (2007), J. Engng. Math. **58**, 317.
- [13] Farhat, M., S. Guenneau, and S. Enoch (2009), Phys. Rev. Lett. **103**, 024301.
- [14] Farhat, M., S. Guenneau, and S. Enoch (2010), European Physics Letters **91**, 54003.
- [15] Farhat, M., S. Guenneau, and S. Enoch (2011), Journal of Computational Physics **230**, 2237.
- [16] Farhat, M., S. Guenneau, S. Enoch, A. Movchan, and G. Petursson (2010), Appl. Phys. Lett. **96**, 081909.
- [17] Graff, K. F. (1975), *Wave motion in elastic solids* (Oxford University Press).
- [18] Greenleaf, A., M. Lassas, and G. Uhlmann (2003), Mathematical Research Letters **10**, 685.
- [19] H., A. H. C. N., F. Guinea, N. M. R. Peres, K. S. Novoselov, and A. K. Geim (2009), Rev. Modern Phys. **81**, 109.
- [20] Harrison, J. M., P. Kuchment, A. Sobolev, and B. Winn (2007), J. Phys. A - Math **40**, 7597.
- [21] Howe, M. S. (1994), Proc. R. Soc. Lond. A **444**, 555.
- [22] Huang, X., Y. Lai, Z. H. Hang, H. Zheng, and C. T. Chan (2011), Nature Materials **10**, 582.
- [23] Kim, S.-H., and M. P. Das (2012), Mod. Phys. Lett. B **26**, 1250105.
- [24] Kittel, C. (1996), *Introduction to solid state physics*, 7th ed. (John Wiley & Sons, New York).
- [25] Kohn, R., H. Shen, M. Vogelius, and M. Weinstein (2008), Inverse Problems **24**, 015016.
- [26] Landau, L. D., and E. M. Lifshitz (1970), *Theory of elasticity*, 2nd ed. (Pergamon Press).
- [27] Liang, Z., and J. Li (2011), Opt. Express **19**, 16821.
- [28] Liu, F., Y. Lai, X. Huang, and C. T. Chan (2011), Phys. Rev. B **84**, 224113.
- [29] Luo, C., S. G. Johnson, and J. D. Joannopoulos (2002), Physical Review B **65**, 201104.
- [30] Mace, B. R. (1996), J. Sound Vib. **192**, 629.
- [31] Mead, D. J. (1996), J. Sound Vib. **190**, 495.
- [32] Movchan, A. B., N. V. Movchan, and R. C. McPhedran (2007), Proc. R. Soc. Lond. A **463**, 2505.
- [33] Murphy, J. E., and G. Li (1994), J. Acoust. Soc. Am. **96**, 2313.
- [34] Nicorovici, N. A., R. C. McPhedran, and L. C. Botten (1995), Phys. Rev. Lett. **75**, 1507.
- [35] Norris, A. N., and G. R. Wickham (1995), Proc. R. Soc. Lond. A **451**, 631.
- [36] Pendry, J. B., A. J. Holden, D. J. Robbins, and W. J. Stewart (1996), Phys. Rev. Lett. **76**, 4773, doi:10.1103/PhysRevLett.76.4773.
- [37] Ramakrishna, S. A. (2005), Rep. Prog. Phys. **68**, 449.
- [38] Stenger, N., M. Wilhelm, and M. Wegener (2012), Phys. Rev. Lett. **108**, 014301.
- [39] Urzhumov, Y., and D. Smith (2010), Phys. Rev. Lett. **105**, 163901.
- [40] Veres, I. A., T. Berer, O. Matsuda, and P. Burgholzer (2012), J. Appl. Phys. **112**, 053504.